

## Research Article

Bo Zhang\* and Song-Sheng Zeng

# Effects of quenching and partitioning (Q&P) technology on microstructure and mechanical properties of VC particulate reinforced wear-resistant alloy

<https://doi.org/10.1515/htmp-2020-0095>

received June 02, 2020; accepted September 21, 2020

**Abstract:** To improve the wear resistance, toughness, and hardness of alloy, the quenching and partitioning (Q&P) technology was applied in the VC particulate (VCp) reinforced wear-resistant alloys, which were prepared by adding different Mn contents (2–5 wt%). The effects of partitioning time on the distribution of alloying elements shown by EDX mapping, retained austenite fraction, microstructure, macro-hardness, and impact toughness were investigated. The results showed that the effect of carbon partitioning time on the hard phase of the wear-resistant alloy was not significant. However, the carbon partitioning time greatly affected the microstructure and the mechanical properties of alloys, such as retained austenite, hardness, and impact toughness, and there was also a strong correlation with the Mn content. When the Mn content was lower (2.51 wt%), the retained austenite content increased with the carbon partitioning time, which resulted in decreased hardness and increased impact toughness. However, when the Mn content was higher (4.52 wt%), the opposite results occurred. This study provided an application of the Q&P technology in a VCp-reinforced wear-resistant alloy.

**Keywords:** Q&P technology, VCp-reinforced phase, wear-resistant alloy, Mn content

## 1 Introduction

Wear-resistant materials have been widely used in modern machinery manufacturing, and conventional wear-resistant

alloys were mainly included high manganese steel [1], nickel-hard cast iron [2], and high-chromium cast iron [3]. Recently, the high-vanadium high-speed alloy has been given much more attention as a result of the increased requirement of increased wear resistance [4]. Cai et al. [5] proposed that the hardness of the VC-reinforced phase was up to 2,600–2,800 Hv, and its particle morphology was superior to the Cr<sub>3</sub>C<sub>7</sub> phase in high-chromium cast iron. To improve the wear resistance of alloys [6–8], the common method was the addition of a large amount of carbon to alloys. However, this method inevitably led to low toughness and plasticity of alloy.

The quenching and partitioning (Q&P) technology [9–12] has been applied to improve the toughness and plasticity of medium and low carbon steels by stabilizing austenite during the martensitic transformation process. This process takes place by the diffusion of carbon from supersaturated martensite obtained at the temperature ranging from  $M_s$  to  $M_f$  by quenching transformation [13,14]. The concentration of carbon in austenite reduces the  $M_s$  temperature and stabilizes untransformed austenite through the proper Q&P process. Thus, the steels treated with the Q&P technology exhibited the excellent toughness and plasticity at the room temperature condition due to the stress and impact energy being partly absorbed during martensite transformation. Choi et al. [15] dealt with the micro-alloyed bar steel using the Q&P technology. The volume fraction of austenite retained at room temperature was mainly dependent on the quenching temperature, partitioning temperature, and partitioning time. Wendler et al. [16] studied Q&P processing with a subzero cooling step and a partitioning step at 450°C. After the Q&P process, the stainless steel exhibited outstanding mechanical properties including yield strength of  $1,050 \pm 12$  MPa, an ultimate tensile strength of  $1,550 \pm 10$  MPa, and a tensile elongation of  $22 \pm 0.3\%$  at room temperature. Huang et al. [17] analyzed the Fe–Cr–C, Fe–Cr–C–Co and Fe–Cr–C–N stainless steels with the Q&P technology. The results showed that about 12% of the total contained carbon in the martensite partitioned into the austenite between 20 and

\* Corresponding author: Bo Zhang, School of Metallurgical and Material Engineering, Hunan University of Technology, Zhuzhou, Hunan 412007, China, e-mail: tale-2002@163.com

Song-Sheng Zeng: School of Metallurgical and Material Engineering, Hunan University of Technology, Zhuzhou, Hunan 412007, China; Hunan Valin Arcelor Mittal Automotive Steel Co., Ltd, Loudi, Hunan 417009, China

200°C, and the formation of tempered carbides was one of the main causes of carbon segregation.

In general, the matrix of the high-vanadium high-speed wear-resistant alloy is mainly martensite [18,19] and includes the slight austenite content. The austenite will be easily transformed to martensite after subsequently tempering. Due to the austenite content being low, the TRIP effect cannot be achieved giving to insufficient toughness. Therefore, the Q&P technology has become a feasible approach for improving the plasticity and toughness of the high-vanadium high-speed wear-resistant alloys. In this study, the high-vanadium high-speed steel wear-resistant alloys with different Mn contents were prepared. To provide a basis for the application of Q&P heat treatment technology in the VC<sub>p</sub>-reinforced wear-resistant alloy, the effects of Q&P technology on the microstructures, as shown by EDX mapping of alloying elements, retained austenite content, and hardness and impact toughness were investigated.

## 2 Material and methods

### 2.1 Preparation of experimental materials

Two types of the VC<sub>p</sub>-reinforced wear-resistant alloy were prepared by adding 3 and 5 wt% Mn, respectively. However, as the Mn element is easy to volatilize and its yield is not stable, the contents of Mn in the final samples are 2.51 and 4.52 wt%. The detailed sample preparation steps are as follows: first, the scrap and pig iron were added in a 50 kg medium-frequency induction furnace for melting, and the slag generated in the melting process was removed. Then, manganese, ferrotitanium, chromium iron, and molybdenum iron were added to the melt, and the aluminum wire was added for deoxygenation when the temperature reached 1,500°C. Later, the vanadium iron alloy was added into the mixed melt. The tapping temperature was controlled at 1,520–1,570°C, and the casting temperature was 1,450–1,480°C. A keel block was cast in

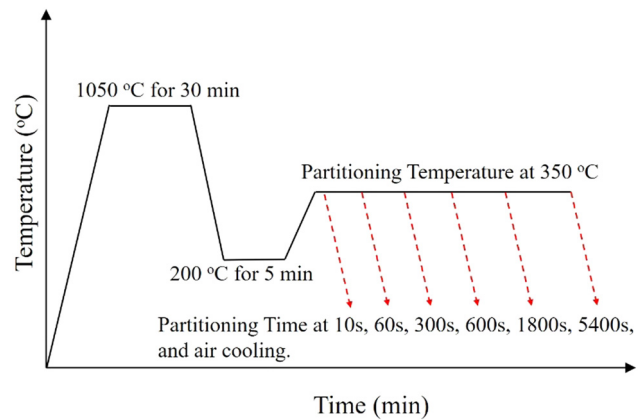


Figure 1: Schematic sketch of the Q&P process.

the sand mold and was removed after cooling. The ingot samples were cut into several specimens of 11 mm × 11 mm × 56 mm in dimensions, and the metallographic specimens of size 10 mm × 10 mm × 15 mm were cut using a wire cutting machine. The compositions of the two types of wear-resistant alloys are presented in Table 1 (the balance was Fe).

### 2.2 The Q&P heat treatment experiment

The effects of the Q&P heat treatment on the structures and properties of two types of wear-resistant alloys were investigated. Figure 1 presented a schematic sketch of the Q&P process, which consisted of isothermal quenching and isothermal carbon partition experiments. For each Mn content alloy (2.51 wt% or 4.52 wt%), six specimens were prepared and put into the furnace together for carrying out the experiment. The quenching temperature was set at 200°C. As the temperature of the current size specimens can reach uniform distribution within 5 min, the holding time was set at 5 min. In the carbon partition process, the temperature was set at 350°C, and six specimens have been taken out in turn for considering the effect of carbon partition time, which were set at 10, 60, 300, 600, 1,800, and 5,400 s.

Table 1: Chemical compositions of experimental alloys (wt%) (Fe balance)

Sample	C	Si	Mn	V	Mo	Cr	Ti	Al	S	P
A1	2.83	0.80	2.51	6.20	1.52	1.83	1.12	0.12	0.05	0.04
A2	2.75	0.79	4.52	6.50	1.47	1.90	1.26	0.14	0.04	0.06

### 2.3 Mechanical property test and microstructure analysis of specimen

After the Q&P heat treatment, the metallographic structure of metallographic specimens were obtained by lycra microscope (DM2700M, Germany) after etched for 20 min at 60°C in a mixture of hydrochloric acid and sulfuric acid. Ingot samples were processed by wire electrical discharge machining into the standard dimensions of 10 mm × 10 mm × 55 mm, and tested for impact toughness in the fall-hammer impact testing machine (JB-100B). Subsequently, the macro hardness values of the samples were measured in a macroscopic Rockwell Hardness Tester (Tester HRS-150) five times, and the averaged value was treated as the final hardness value. In addition, the microstructure of sample was obtained by scanning electron microscope (SEM; SIGMA 300, Germany) operating at 30 kV, and its retained austenite fraction was measured by X ray diffraction (XRD; Philips-X'Pert Pro MPD, Holland) with Cu  $\kappa_1$  radiation (1.540598 Å). After determining the position of Bragg peaks observed over the range of  $2\theta = 5\text{--}90^\circ$ , the phases were identified using databases of the International Centre for Diffraction Data, and the austenite proportion was calculated by [20,21]:

$$W_a = \frac{I_a}{I_a + I_b/(K_b/a)} \quad (1)$$

where  $W_a$  = mass fraction of retained austenite (wt%),  $I_a$  = diffraction peak height of retained austenite,  $I_b$  = diffraction peak intensity of matrix, and  $K_b/a$  = integral height ratio of the strongest diffraction peaks between retained austenite and matrix.

## 3 Results and discussion

### 3.1 Effects of the Q&P technology on the microstructure and elements mapping

The microstructures of two types of specimens with different Mn contents were shown in Figure 2. The black particles presented the hard phase ( $VC_P$ ), and the gray area around the hard phase was matrix. Figure 2(a) shows that the distribution of  $VC_P$  was nonuniform when the Mn content was low (2.51 wt%). The distribution of  $VC_P$  in red frame was sparse, whereas its distribution in the blue frame was denser. However, when the Mn content was high (4.52 wt%), the distribution of  $VC_P$  tended to be more uniform, as shown in Figure 2(b).

Figures 3(a), 4(a), and 5(a) were SEM-BSE images. The gray parts of the alloy were matrix, and the black parts present the hard phase. Figures 3(b–f), 4(b–f), and 5(b–f) show the element mapping of the A1 alloy at different partition times. All of V formed the carbide hard phase at different partition times. Ti was also a main element in the hard phase, and it was enriched in the center of the hard phase. However, with an increase in the partition time, a very slight amount of Ti diffused to the matrix. Compared with V and Ti, the amounts of Cr and Mo, which were enriched in hard phase, were smaller, and more of Cr and Mo diffused from the hard phase to the matrix with the increased partition time. When the partition time was 5,400 s, the diffusion phenomenon of Mo was significant because V, Ti, Cr, and Mo have different stabilities in carbides. The stability of carbides in alloy depends on the number of electrons in the d-layer of the element [22,23]. The lower the number of d-layer electrons

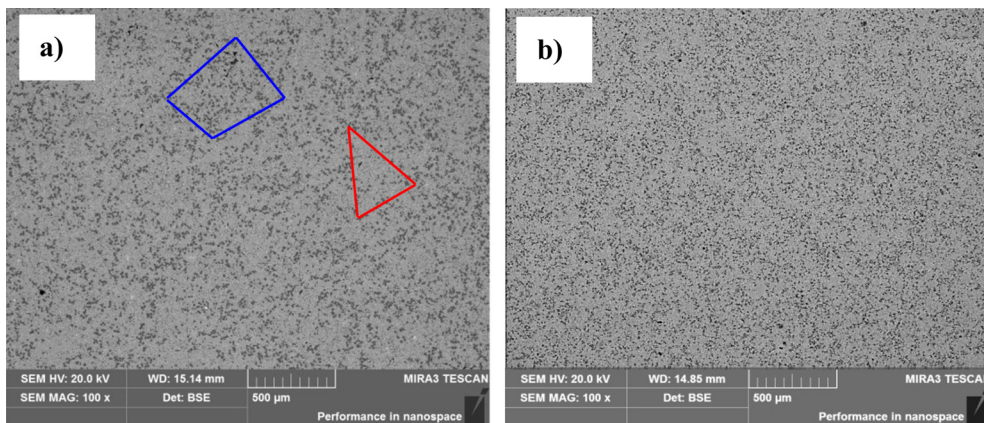


**Figure 2:** SEM-BSE images showing microstructures of as-cast samples: (a) 2.51 wt% Mn and (b) 4.52 wt% Mn, and black particles are the precipitates of VC.

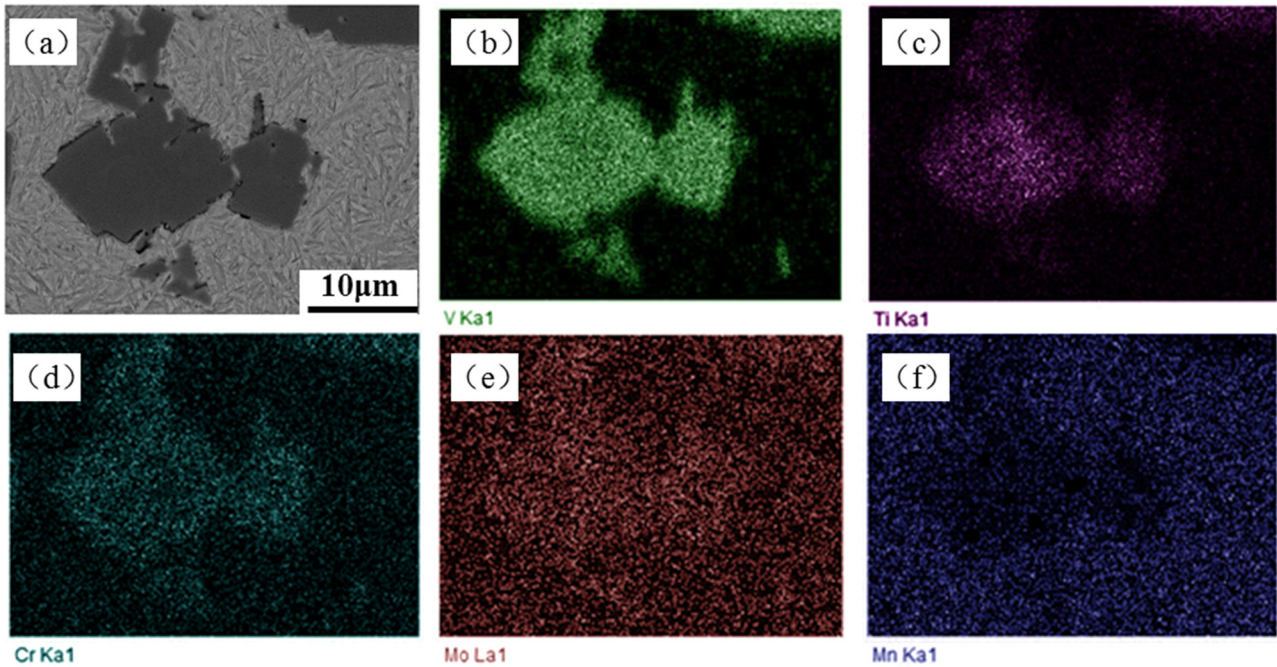


**Figure 3:** Elemental maps of A1 alloy for 60 s partitioning time: (a)-SEM-BSE image and EDX map for (b) V, (c) Ti, (d) Cr, (e) Mo, and (f) Mn.

of the alloy element, the more stable the precipitated carbides. The order of d-layer electrons number is  $Ti(2) < V(3) < Cr(4) < Mo(5)$  [23]. Therefore, compared with Cr and Mo, V and Ti more tended to form carbides, and their distributions in the hard phase were more stable. With the increased

partition time, the slight diffusion of Ti from the hard phase to the matrix may be caused by the combination of Ti and N in the matrix [24]. However, Mn was mainly distributed in the matrix. This was because the carbide of Mn was unstable, and Mn has a strong binding force with Fe [23].

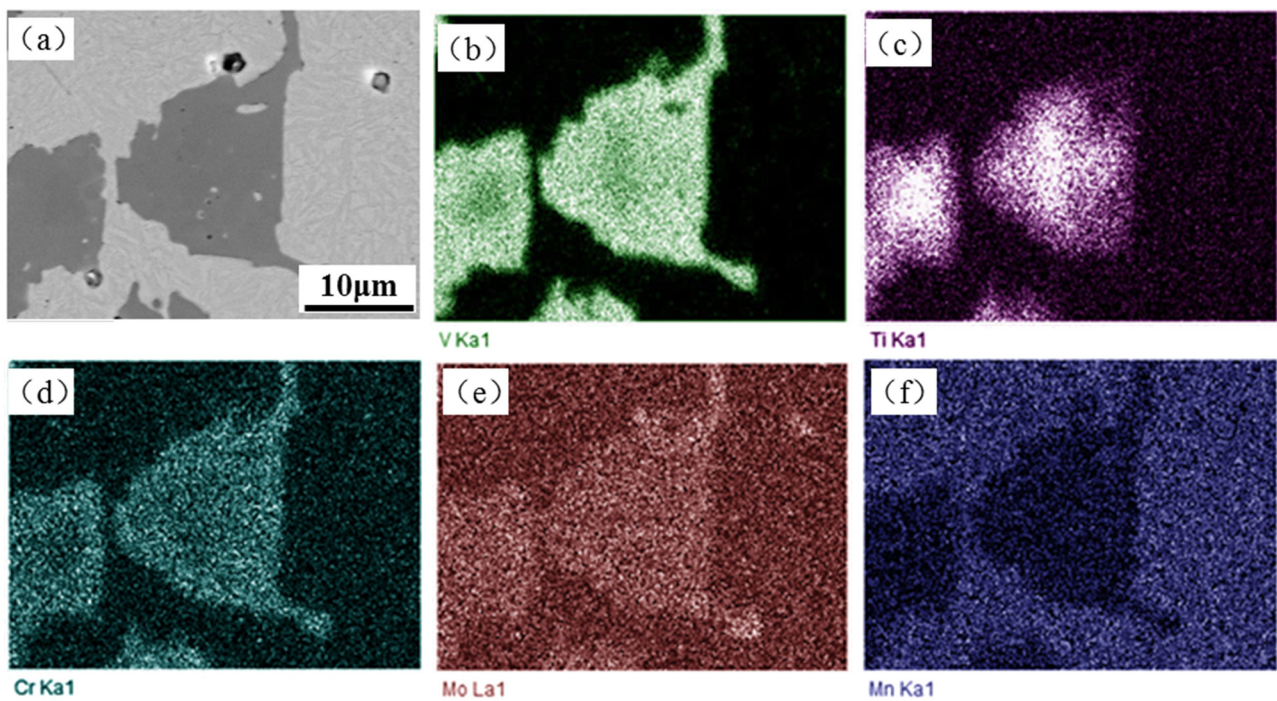


**Figure 4:** Elemental maps of A1 alloy for 1,800 s partitioning time: (a)-SEM-BSE image and EDX map for (b) V, (c) Ti, (d) Cr, (e) Mo, and (f) Mn.

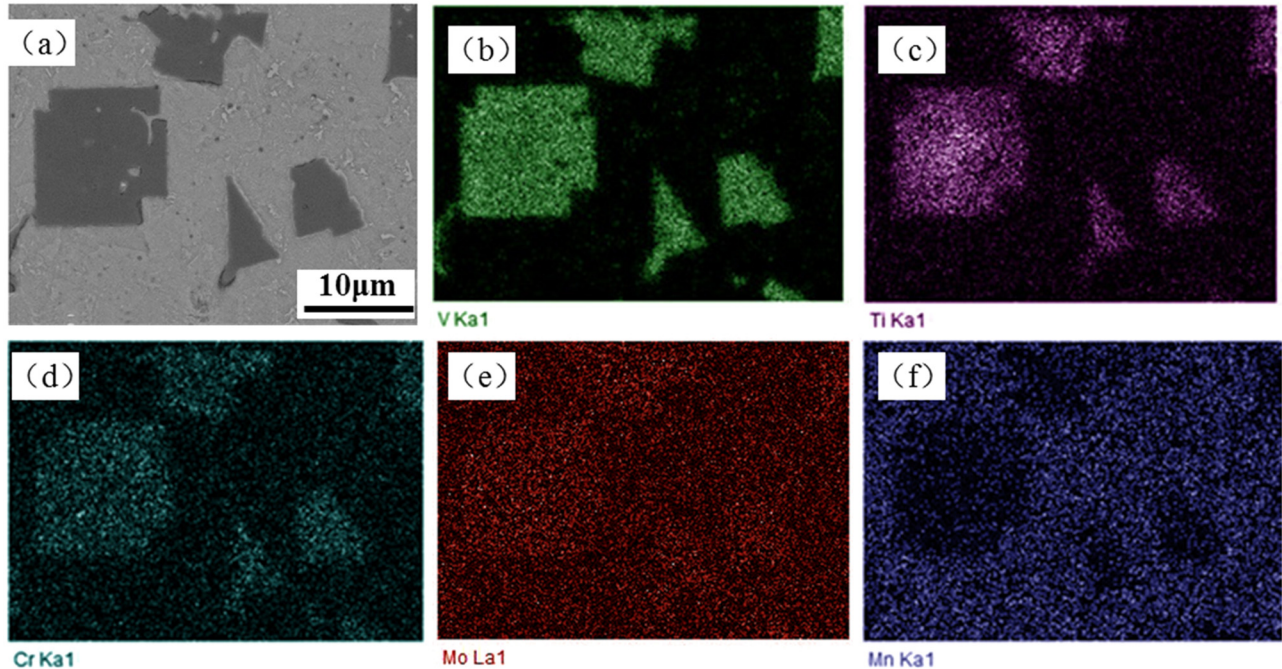


**Figure 5:** Elemental maps of A1 alloy for 5,400 s partitioning time: (a)-SEM-BSE image and EDX map for (b) V, (c) Ti, (d) Cr, (e) Mo, and (f) Mn.

It ensured that the hardness of the hard phase did not greatly change during the Q&P process.

### 3.2 Effect of partition time on retained austenite

The results of XRD with different Mn contents are shown in Figure 6, and the mass fraction of austenite calculated using equation (1) was presented in Table 2. The retained austenite content in alloy A1 increased from 9.3 to 15.6 wt% with the increased partition time. As the Mn content increased, the retained austenite content in alloy A2 was high at the 60 s partition time, but it decreased to 34.10 wt% with the longer partition time. This was due to the retained austenite decomposing with the increasing of partition time [25,26]. However, the final retained austenite content was higher for the larger Mn addition.

### 3.3 Effect of Q&P technology on hardness and impact toughness

Figure 7(a) shows the hardness changes of alloy A1 and alloy A2 with different carbon partition times, and Figure 7(b)

shows the microstructures of two alloys at different carbon partition times, where points (a), (b), (c), and (d) corresponded to the points on Figure 7(a). Figure 7(a) shows the hardness changes of these two alloys had the opposite trends. When the Mn content was 2.51 wt% (alloy A1), the initial hardness of alloy A1 was high. This was due to the martensite content in alloy A1 being relatively high, which can be clearly seen in point (a) of Figure 7(b). Due to the martensite changing to austenite point (b) of Figure 7(b)), the hardness of alloy A1

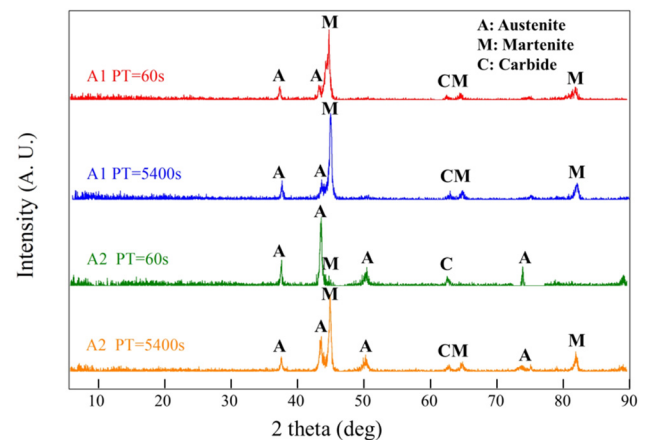
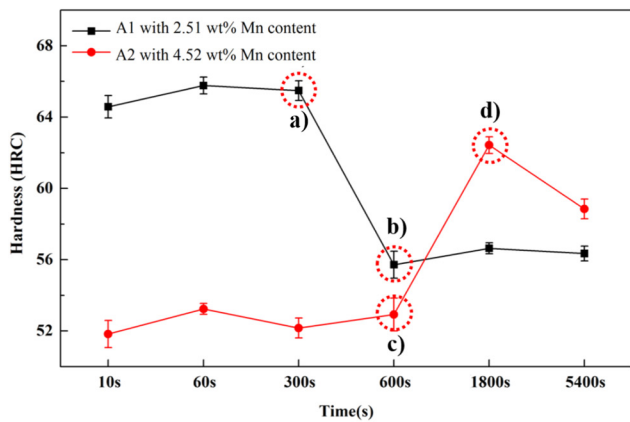


**Figure 6:** Retained austenite spectrum by XRD.

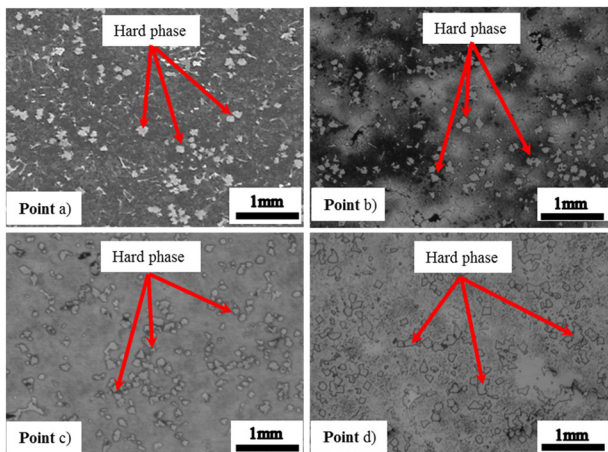
**Table 2:** Retained austenite fraction of wear-resistant alloys (volume, %)

Alloys	Mn (wt%)	Partition time (s)	Austenite fraction
A1	2.51	60	9.3
	2.51	5,400	15.6
A2	4.52	60	85.8
	4.52	5,400	34.1

decreased sharply from  $(66 \pm 0.32)$  HRC to  $(56 \pm 0.41)$  HRC with the increased carbon partition time. For the alloy A2 (Mn = 4.52 wt%), the initial hardness was lower than that of alloy A1. This was because the martensite was low before 600 s, and the austenite was the main phase, as shown in point (c) of Figure 7(b). However, the hardness



(a)



(b)

**Figure 7:** Hardness and microstructures of alloys A1 and A2 with different carbon partition times. (a) Hardness change of alloys A1 and A2 with different carbon partition times. (b) Metallographic structure of alloys A1 and A2 with different carbon partition times. In this figure, the particles present the hard phase, the black areas around particles were martensite, and the gray areas around particles were austenite.

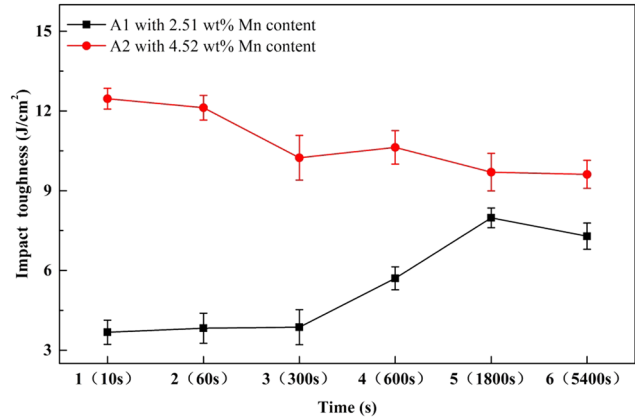


**Figure 8:** Impact toughness changes of alloys A1 and A2 with different carbon partition times.

of alloy A2 increased with the increased partition time, especially at point (d). This was because some of austenite changed to the martensite during the later carbon partition process.

Figure 8 shows the impact toughness changes of alloys A1 and A2 with different carbon partition times. The Q&P technology had different effects for the different Mn contents. The impact toughness of alloy A1 had an overall increase with the increased the carbon partition time, whereas the trend of alloy A2 was decreased. The impact toughness of alloy was affected by the austenite content, and the results matched well with the aforementioned analyses.

## 4 Conclusions

In this study, two types of VC<sub>p</sub>-reinforced wear-resistant alloys with different Mn contents were used to investigate the effects of Q&P heat treatment technology on the alloy performances. The main conclusions are as follows:

- (1) Compared to the lower Mn content condition (2.51 wt%), the distribution of VC<sub>p</sub> had uniform distribution when the Mn content was higher (4.52 wt%).
- (2) The hard phases were carbides of Ti, V, Cr, and Mo, while the Mn element was mainly distributed in the matrix. Therefore, the hardness of the hard phase had no great change during the Q&P process.
- (3) The carbon partitioning time had a significant effect on the retained austenite fraction of alloy, and its effect varied with the Mn content. In general, the element of Mn increased the austenite content in alloy, resulting in the higher impact toughness of alloy.

**Acknowledgments:** The authors gratefully acknowledge the financial support for this work from the Specialized Research Fund for the National Natural Science Foundation of China (No. 51504090) and the Natural Science Foundation of Hunan Province, China (No. 2019JJ60062).

**Data availability statement:** The data used to support the findings of this study are available from the corresponding author upon request.

## References

- [1] Zhang, X. Z., F. Ni, S. Z. Wei, R. Long, and Y. P. Ji. The effects of potassium salt multi-modification on carbide morphologies and distribution of high vanadium high speed steel. *Foundry*, Vol. 56, 2007, pp. 290–293.
- [2] Li, P., Z. Z. Du, H. G. Fu, and Z. J. Feng. Effect of heat treatment temperature on microstructure and hardness of high vanadium high speed steel. *Materials for Mechanical Engineering*, Vol. 33, 2009, pp. 93–95.
- [3] Xu, L., Z. Yan, and Y. Liu. Microstructure evolution and martensitic transformation behaviors of 9Cr–1.8W–0.3Mo ferritic heat-resistant steel during quenching and partitioning treatment. *The Journal of Materials Research*, Vol. 28, 2013, pp. 2835–2843.
- [4] Seo, E. J., L. Cho, and Y. Estrin. Microstructure-mechanical properties relationships for quenching and partitioning (Q&P) processed steel. *Acta Materialia*, Vol. 113, 2016, pp. 124–139.
- [5] Cai, B., Y. F. Tan, H. E. Long, H. Tan, and X. L. Wang. Tribological behavior and mechanisms of graphite/CaF<sub>2</sub>/TiC/Ni-base alloy composite coatings. *Transactions of Nonferrous Metals Society of China*, Vol. 23, 2013, pp. 392–399.
- [6] Lee, S., S. J. Lee, and B. C. De Cooman. Austenite stability of ultrafine-grained transformation-induced plasticity steel with Mn partitioning. *Scripta Materialia*, Vol. 65, 2011, pp. 225–228.
- [7] Liu, G., S. G. Zhang, Q. G. Meng, J. Wang, and J. Li. Integrated treatment of GCP and slag quenching water of LD steel making unit. *Ironmaking & Steelmaking*, Vol. 44, 2017, pp. 1–8.
- [8] Speer, J., D. K. Matlock, and B. C. D. Cooman. Carbon partitioning into austenite after martensite transformation. *Acta Materialia*, Vol. 51, 2003, pp. 2611–2622.
- [9] Speer, J. G., D. V. Edmonds, and F. C. Rizzo. Partitioning of carbon from supersaturated plates of ferrite, with application to steel processing and fundamentals of the bainite transformation. *Current Opinion in Solid State & Materials Science*, Vol. 8, 2004, pp. 219–237.
- [10] He, B., J. Li, C. B. Shi, and H. Wang. Effect of cooling intensity on carbides in Mg-containing H13 steel during the electroslag remelting process. *Chinese Journal of Engineering*, Vol. 38, 2016, pp. 1720–1727.
- [11] Zhong, N., Q. Wu, and Y. Yin. Microstructural evolution of a medium carbon advanced high strength steel heat-treated by Quenching-Partitioning Process. *Steel Research International*, Vol. 86, 2015, pp. 252–256.
- [12] Liu, H. F., Y. H. Liu, and S. R. Yu. Investigation of the wear resistance of high carbon high vanadium high speed steel. *Tribology*, Vol. 20, 2000, pp. 401–406.
- [13] Matlock, D. K., and J. G. Speer. *Third Generation of AHSS: Microstructure Design Concepts*. Springer, London, 2009, pp. 185–205.
- [14] Xu, L., Z. Yan, and Y. Liu. Microstructure evolution and martensitic transformation behaviors of 9Cr–1.8W–0.3Mo ferritic heat-resistant steel during quenching and partitioning treatment. *The Journal of Materials Research*, Vol. 28, 2013, pp. 2835–2843.
- [15] Choi, I., D. M. Bruce, D. K. Matlock, and J. G. Speer. The high speed deformation behavior of TRIP steels. *Metals & Materials International*, Vol. 14, 2008, pp. 139–146.
- [16] Wendler, M., C. Ullrich, M. Hauser, L. Krüger, O. Volkova, A. Weiß, et al. Quenching and partitioning (Q&P) processing of fully austenitic stainless steels. *Acta Materialia*, Vol. 133, 2017, pp. 346–355.
- [17] Huang, Q., C. Schröder, H. Biermann, O. Volkova, and J. Mola. Influence of Martensite Fraction on Tensile Properties of Quenched and Partitioned (Q&P) Martensitic Stainless Steels. *Steel Research International*, Vol. 87, 2016, pp. 1082–1094.
- [18] Clarke, A. J., J. G. Speer, and M. K. Miller. Carbon partitioning to austenite from martensite or bainite during the quench and partition (Q&P) process: A critical assessment. *Acta Materialia*, Vol. 56, 2008, pp. 16–22.
- [19] Clarke, A. J., J. G. Speer, and D. K. Matlock. Influence of carbon partitioning kinetics on final austenite fraction during quenching and partitioning. *Scripta Materialia*, Vol. 61, 2009, pp. 149–152.
- [20] Edmonds, D. V., K. He, and F. C. Rizzo. Quenching and partitioning martensite—A novel steel heat treatment. *Materials Science and Engineering: A*, Vol. 25, 2006, pp. 25–34.
- [21] Cho, L., E. J. Seo, and B. C. De Cooman. Near-Ac3 austenitized ultra-fine-grained quenching and partitioning (Q&P) steel. *Scripta Materialia*, Vol. 123, 2016, pp. 69–72.
- [22] Sluiter, M. Phase Stability of Carbides and Nitrides in Steel. *Materials Research Society Proceedings*, Vol. 979, 2006, pp. 3–8.
- [23] Yu, X. X., C. R. Weinberger, and G. B. Thompson. Ab initio investigations of the phase stability in group IVB and VB transition metal carbides. *Computational Materials Science*, Vol. 112, 2016, pp. 18–326.
- [24] Yugeswaran, S., A. Kobayashi, K. Suresh, and B. Subramanian. Characterization of gas tunnel type plasma sprayed TiN reinforced Fe-based metallic glass coatings. *Journal of Alloys and Compounds*, Vol. 551, 2013, pp. 168–175.
- [25] Zhu, S., S. Kuang, and Y. Jiang. Effect of quenching and partitioning process on microstructure and mechanical properties of Q&P steel. *Jinshu Rechuli/Heat Treatment of Metals*, Vol. 38, 2013, pp. 1–4.
- [26] Zhou, Y., and G. Zhang. Study on electronic theory of the interaction between rare earth elements and impurities at grain boundaries in Ni-base superalloy. *Rare Metal Materials & Engineering*, Vol. 36, 2007, pp. 2160–2162.